IOP Publishing and International Atomic Energy Agency Nuclear Fusion
Nucl. Fusion **49** (2009) 075021 (6pp) doi:10.1088/0029-5515/49/7/075021

Kinetic analysis of the resistive wall modes in the ITER advanced tokamak scenario

L.J. Zheng, M.T. Kotschenreuther and J.W. Van Dam

Institute for Fusion Studies, University of Texas at Austin, Austin, TX 78712, USA

Received 1 January 2009, accepted for publication 12 May 2009
Published 8 June 2009
Online at stacks.iop.org/NF/49/075021

Abstract
It is found that $n = 1$ resistive wall modes in the ITER advanced scenario can be fully stabilized by modestly low rotation with a rotation frequency (normalized to the Alfvén frequency at the magnetic axis) of about $\Omega = 0.0075$. The existence of this stabilization scheme is proved with the AEGIS-K (Adaptive EiGenfunction Independent Solution-Kinetic) code, which provides a fully kinetic (non-hybrid) and self-consistent (non-perturbative) description of the system. Wave-particle resonances, shear Alfvén continuum damping, trapped particle effect and the parallel electric effects are all taken into account. The rotation frequency for full stabilization is much larger than the diamagnetic drift frequency; therefore, finite Larmor radius effects are negligible. We also find that the rotation stabilization window opens first near the ideal wall limit.

PACS numbers: 52.35.Py, 52.55.Fa, 52.55.Hc

1. Introduction

Resistive wall mode stability [1] is a major concern for ITER. It has been shown previously that the kinetic and Alfvén resonances can play significant roles in stabilizing the resistive wall modes [2–6]. However, a fully kinetic analysis of the resistive wall modes is a challenging issue. First, the conventional gyrokinetic equation cannot recover magnetohydrodynamics (MHD), and most existing kinetic MHD codes are hybrid in nature. Second, the coupling of Alfvén continuum damping requires high-resolution computation of the modes at the singular surfaces, which is difficult to achieve with the usual non-adaptive codes. Even in the hybrid scheme, it is unclear how the kinetic and Alfvén resonances are coupled and how the parallel electric field affects the stability. All of these issues point to the need for a systematic kinetic analysis of the resistive wall modes in ITER.

Our current effort aims to resolve these difficulties by developing a fully kinetic analysis of the resistive wall modes in ITER. To achieve this goal, the theoretical formalism should, on the one hand, be based on first principles and therefore must be non-hybrid; and on the other hand, should be numerically implementable. Our approach is to derive an extended gyrokinetic formalism that can recover the MHD limit. Our achievement of the recovery of MHD from our newly developed gyrokinetics [9] enables us to extend the MHD stability analyses directly to a fully kinetic analysis without invoking the hybrid kinetic-fluid hypothesis.

Recovering the MHD equations from gyrokinetics is not trivial. We find that the conventional gyrokinetic formalism [7, 8] needs to be significantly modified in order to maintain consistency of ordering and recover the MHD limit [9]. Several major modifications need to be made simultaneously: (1) a sufficiently high-order equilibrium distribution function must be used; (2) the gyrophase-dependent part of the perturbed distribution function and its coupling to the gyrophase-independent part of the perturbed distribution function should be included and (3) the adiabatic invariants should be computed to sufficient order. Our newly developed gyrokinetic theory in [9] modifies the conventional theory in several important aspects: for example, we recover the Pfirsch–Schlüter current effect in the perpendicular momentum equation and the missing finite Larmor radius (FLR) effects. Especially we have shown that the conventional results about the FLR effects based on the introduction of the Bessel functions J_0 and J_1 are incomplete in general. Even at lowest order our gyrophase-averaged gyrokinetic equation is different from the conventional drift kinetic equation. This is due to the coupling of the gyrophase-dependent part of the distribution function to the gyrophase-averaged gyrokinetic equation.

The success in recovering full MHD with our newly derived gyrokinetic theory now allows the possibility to consistently study the stability of resistive wall modes in a non-hybrid manner. In this work we neglect the FLR effects and focus on the particle-wave resonances, the continuum damping, the trapped particle effect and the parallel electric field effects. We numerically implement our newly developed gyrokinetic theory by extending our existing AEGIS [11] to the AEGIS-K kinetic version [12]. With the kinetic effect and the coupling of the shear Alfvén resonances taken into account, we

are able to study rotation stabilization of resistive wall modes in an ITER advanced tokamak scenario.

The paper is arranged as follows. In section 2, the theoretical formalism and the AEGIS-K code are described; in section 3, the numerical investigation of resistive wall modes in the ITER advanced tokamak scenario is presented; in the last section, conclusions and discussion are given.

2. Theoretical formalism and AEGIS-K code

We use our newly developed gyrokinetic formalism in [9] for this investigation. Having recovered the MHD from this formalism, we are able to study the MHD modes in a non-hybrid manner. For simplicity, we drop the FLR effects in our first effort. Even in this limit our starting equations are different from those of the conventional drift kinetic formalism. In the conventional derivation of the drift kinetic equation, the coupling between the gyrophase-averaged part and the gyrophase-dependent part of the gyrokinetic distribution function through the term $\dot{\alpha}_1 \partial \delta f/\partial \alpha$ has not been taken into account. Here, δf is the distribution function and α is the gyrophase, with the subscript '1' denoting the first order and the dot representing the time derivative along the unperturbed particle orbit. Actually, only if this coupling is taken into account can the parallel MHD equation of motion be retrieved in the proper limit. This coupling can be, alternatively, taken into account by including α_1 into the generalized gyrophase definition.

The basic set of equations is as follows: the perpendicular momentum equation

$$-\rho_{\mathrm{m}}\hat{\omega}^2\boldsymbol{\xi} = \delta\boldsymbol{J}\times\boldsymbol{B} + \boldsymbol{J}\times\delta\boldsymbol{B} - \boldsymbol{\nabla}\delta P_{\mathrm{c}} - \boldsymbol{\nabla}_\perp \int \mathrm{d}^3 v (m_\rho \mu B)\delta f_0(\boldsymbol{x}), \tag{1}$$

the gyrophase-independent part of the gyrokinetic equation

$$v_\parallel \cdot \boldsymbol{\nabla} f_0(\boldsymbol{X}) - \mathrm{i}\hat{\omega}\delta f_0(\boldsymbol{X}) = \mathrm{i}\hat{\omega}\frac{m_\rho}{T_{\mathrm{i}}}\mu B F_{g0}\boldsymbol{\nabla}_\perp\cdot\boldsymbol{\xi} + \mathrm{i}\hat{\omega}\frac{m_\rho}{T_{\mathrm{i}}}(\mu B - v_\parallel^2)F_{g0}\boldsymbol{\kappa}\cdot\boldsymbol{\xi} - \mathrm{i}\hat{\omega}\frac{Ze_{\mathrm{i}}}{T_{\mathrm{i}}}F_{g0}\delta\varphi, \tag{2}$$

and the quasineutrality condition

$$\delta\varphi = -\frac{1}{1+Z\tau}\frac{T_{\mathrm{e}}}{Ze_{\mathrm{i}}}\frac{1}{n_0}\int \mathrm{d}^3 v \delta f_{0\mathrm{i}}. \tag{3}$$

Here, ρ_{m} is the mass density, m_ρ denotes the mass, e_{i} is the ion charge, Z is the charge number, n_0 is the ion density, $\boldsymbol{\xi}$ is the perpendicular field line displacement, $\boldsymbol{B}$ denotes the equilibrium magnetic field, $\delta\boldsymbol{B} = \boldsymbol{\nabla}\times\boldsymbol{\xi}\times\boldsymbol{B}$, $\delta\boldsymbol{J} = \boldsymbol{\nabla}\times\delta\boldsymbol{B}$, P represents the equilibrium pressure, $\delta P_{\mathrm{c}} = -\boldsymbol{\xi}\cdot\boldsymbol{\nabla}P$, v is the ion speed, $\mu = v_\perp^2/2B$ is the magnetic moment, T represents the temperature, $\tau = T_{\mathrm{i}}/T_{\mathrm{e}}$ with subscripts i and e represents, respectively, the ion and electron species, $\boldsymbol{\kappa}$ represents the field line curvature, $\delta\varphi$ specifies the parallel electric field effect, $\delta f_{0\mathrm{i}}$ denotes the gyrophase averaged distribution function for ion species, F_g is the Maxwellian distribution function and the subscripts $\perp$ and $\parallel$ represent, respectively, the perpendicular and the parallel components to the equilibrium magnetic field line. Due to the low mode frequency, we have assumed the electron response to be adiabatic. We consider only the rotation to be low as it is more interested for ITER. We then include the rotation effects by replacing the mode frequency ω with $\hat{\omega} \equiv \omega + n\Omega$ in equations (1)–(3), where Ω is the rotation frequency. Note that the source terms on the right hand side of equation (2) are different from those of the conventional drift kinetic equation.

Here, we discuss the reason for our inclusion of the rotation effects only by the Doppler shift in our formalism. In actuality, rotation effects enter into the problem in three categories—that is, not only through the Doppler shift, but also via centrifugal force and Coriolis force. We investigate the case when the rotation speed is much less than the ion thermal speed. For this case, it can be shown that the rotation effects of centrifugal force and Coriolis force are negligibly small. In the ideal MHD case, this has been demonstrated in [10]. In the kinetic description, we note, however, that when one stays in the rotating frame of reference, it can be shown that the centrifugal and Coriolis forces in this frame result from the rotation, and since the rotation speed is much smaller than the thermal speed, therefore particle drifts due to the rotation speed are likewise smaller than those due to the thermal speed. Consequently, only the Doppler shift effect from rotation remains.

In our set of equations the wave–particle resonances, the shear Alfvén continuum damping, the trapped particle effect and the parallel electric effects are all taken into account. We have not considered the precessional drift resonance as [5], since we note that considering the resonance alone is insufficient for ordering consistency. Since $\langle\omega_{\mathrm{d}}\rangle/\omega_{*\mathrm{i}} \sim a/R$, inclusion of the $\langle\omega_{\mathrm{d}}\rangle$ effect also needs to take into account the $\omega_{*\mathrm{i}}$ effect (i.e. $k_\perp^2\rho_{\mathrm{i}}^2$ effects) for consistency. Here, $\langle\omega_{\mathrm{d}}\rangle$ is the processional drift frequency, $\omega_{*\mathrm{i}}$ is the ion diamagnetic drift frequency, $k_\perp$ represents the perpendicular wave number and ρ_{i} is the ion gyro radius. Due to this complexity, we postpone this part of the work to future studies.

We implement our newly derived set of equations (1)–(3) by extending our existing AEGIS [11] to the AEGIS-K code. In AEGIS-K formalism, the Fourier decomposition is employed in the poloidal direction. In the radial direction, the decomposition using the independent solutions are used, instead of using the finite element decomposition as the conventional codes. The independent solutions are obtained by adaptive numerical shooting. To apply this method for global eigen mode calculation, one has to overcome the difficulty induced by the numerical pollution due to the large solution associated with independent solutions. To solve this difficulty AEGIS formalism uses the multiple region matching method, which has shown to be successful in the ideal MHD calculation in [11]. We also find that this method works well for the kinetic case [12]. Since the AEGIS formalism is based on the adaptive numerical scheme, we are able to resolve the coupling between the kinetic and the shear Alfvén resonances.

3. Numerical investigation of resistive wall modes in ITER configuration

We consider an ITER advanced tokamak configuration and the $n = 1$ resistive wall modes, where n is the toroidal mode number. The numerical equilibrium is generated by the TOQ code (the MHD equilibrium code developed at General Atomics, San Diego, CA). The typical parameters (for

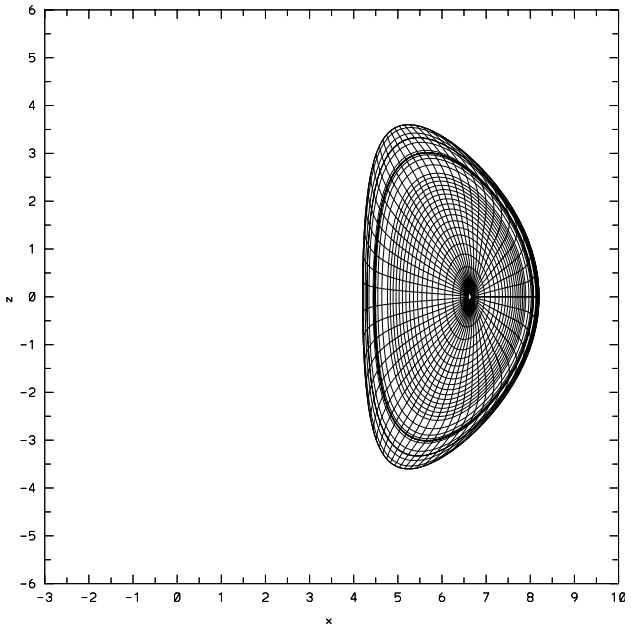

Figure 1. Cross section of the ITER advanced tokamak configuration with poloidal and radial packed grids shown. The poloidal coordinates shown here are the Hamada coordinate.

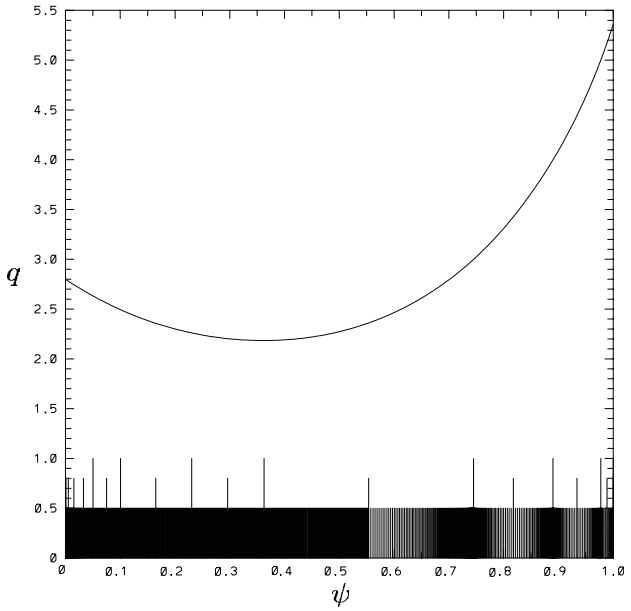

Figure 2. Typical safety factor profile, with the maximum step size and the region separation for matching shown.

$\beta_N = 3.2$) are as follows: $q_0 = 2.8$, $q_a = 5.36$, $q_{min} = 2.18$, $q_{95} = 4.20$, elongation elongation $\kappa_a = 1.8$, and triangularity $\delta_a = 0.48$. Here, q_0, q_a, q_{min}, and q_{95} are, respectively, the safety factor values at the magnetic axis, the plasma edge, the q minimum and the 95% radial flux surface. The rotation profile is specified as $\Omega(1 - \psi^2)$. We consider the conformal wall at the current calculation and assume the equilibrium to be up–down symmetric. The plasma cross section is given in figure 1. The typical safety factor profile (for $\beta_N = 3.2$) is shown in figure 2. Also shown in figure 2 is the radial grid for eigen function output and the region separation for matching.

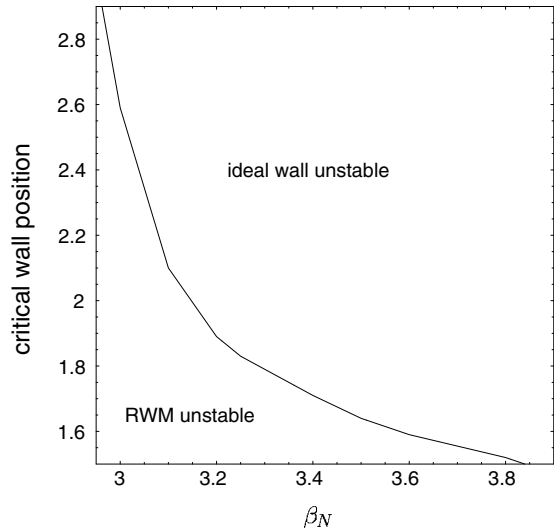

Figure 3. The critical wall position for ideal MHD resistive wall modes versus the beta normal β_N. There is no rotation in this case.

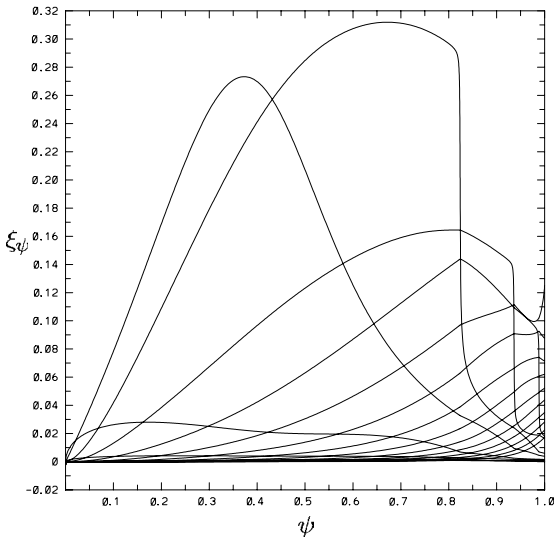

Figure 4. Fourier components of radial field line displacement versus the radial coordinate ψ for typical unstable resistive wall modes without rotation, as computed by AEGIS. The beta normal is $\beta_N = 3.2$.

For baseline reference we first compute the case without rotation with AEGIS code. Note that the AEGIS-K code converges to the AEGIS results as the rotation and kinetic effects are taken away. We also note that the AEGIS code is in complete agreement with GATO [13] for ideal MHD computations [9]. Figure 3 shows the ideal MHD stability boundary for the critical wall position b (normalized by the minor radius) versus the beta normal $\beta_N (\equiv \beta(I/aB_0)^{-1})$, where β is the ratio of the plasma to the magnetic energies, I represents the tokamak toroidal current, a is the minor radius, and B_0 denotes the magnetic field at the magnetic axis. As usual [1], the unstable resistive wall modes are recovered in the ideal wall stabilization region. The typical ideal MHD eigen mode is shown in figure 4.

With rotation and kinetic effects included, we find that the stability boundary changed and the rotation and

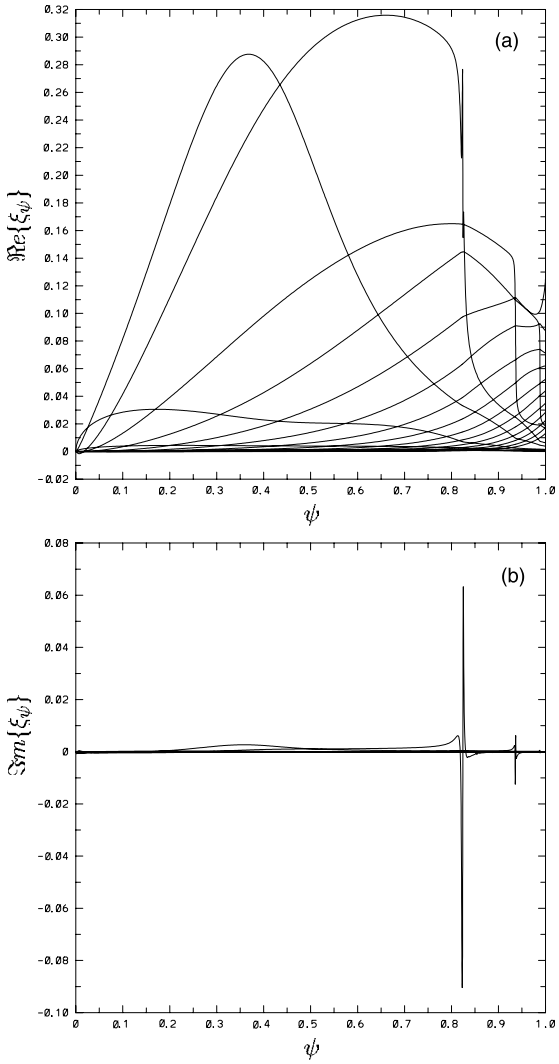

Figure 5. Real (a) and imaginary (b) parts of the Fourier components of radial field line displacement versus the radial coordinate ψ for the unstable resistive wall mode in the presence of rotation and kinetic effects. The equilibrium parameters are as follows: $\beta_N = 3.2$, $\Omega = 0.003$ and $b = 1.5$.

kinetic stabilization channel appears. A typical unstable kinetic mode computed by the AEGIS-K code is given in figure 5 for beta normal $\beta_N = 3.2$ and normalized rotation frequency $\Omega = 0.003$. Note that in this presentation, the rotation frequency Ω is normalized by the Alfvén speed $\sqrt{B^2/(\mu_0 \rho_m R^2 q^2)}$ at the magnetic axis. Here, R is the major radius and μ_0 is the magnetic constant. One of the advantages of the AEGIS-K code lies in that it preserves the ideal MHD roots. This can be seen from a comparison between figure 4 and 5(a).

Figure 6 shows the resistive wall mode growth rate $\gamma\tau_w$ versus the wall position b for fixed beta value $\beta_N = 3.2$. Here, the wall time $\tau_w = \mu_0 \sigma d \bar{b}$ is introduced to scale the resistive wall mode growth rate, where σ is wall conductivity, d is wall thickness and $\bar{b}$ is average wall minor radius. From this figure one can see that the rotation and kinetic stabilization channel appears first near the critical wall limit as rotation increases. This feature also occurs in the stability diagram for the resistive wall mode growth rate versus the beta normal β_N as will be

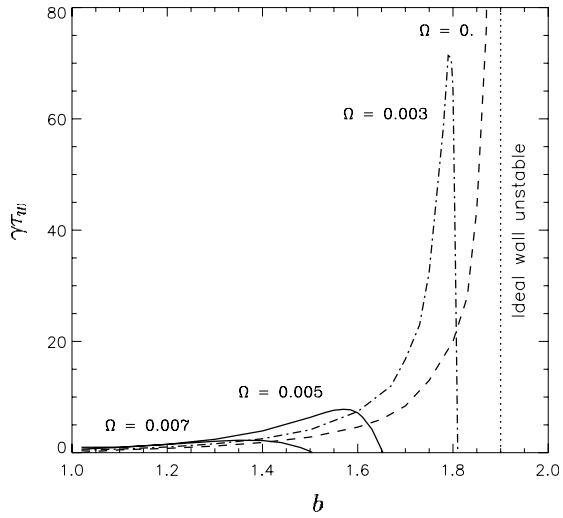

Figure 6. Resistive wall mode growth rate versus the wall position for beta normal $\beta_N = 3.2$, as computed by the AEGIS-K code. The dashed curve represents the growth rate without plasma rotation and kinetic effects. The dashed–dot ($\Omega = 0.003$), dashed–dot–dot ($\Omega = 0.005$) and solid ($\Omega = 0.007$) curves are the growth rates with plasma rotation and kinetic effects included.

discussed later in this paper. Comparison with the results in [4] shows the effects found in the current kinetic computation is not purely due to the Alfvén continuum damping. Nevertheless, we note that the equilibrium in [4] (Ohmic scenario) is different from the current one. However, the apparent order-of-magnitude difference in rotation frequency is not due to the difference in equilibria. Note that the results in [4] are for an incompressible plasma in the parallel direction. The plasma parallel compressibility can give rise to the so-called apparent mass effect, given by the factor $(1 + 2q^2)$. Therefore, the actual rotation frequency in [4] is in fact one order of magnitude smaller, and is therefore on the same order as the current results. This shows the consistency of our work, since the kinetic computation in this paper corresponds to a compressible plasma in the parallel direction.

To study the dependence of the resistive wall mode stability on the beta value, we consider a series of numerical equilibria with beta normal values ranging from the no wall limit $\beta_N^{\text{no wall}} = 2.95$ to the ideal wall limit $\beta_N^{\text{ideal wall}} = 3.84$ for fixed wall position $b = 1.5$. Figure 7 shows the resistive wall mode growth rate versus the normalized beta C_β for a given wall position $b = 1.5$. As usual, the normalized beta is defined as follows:

$$C_\beta = \frac{\beta_N - \beta_N^{\text{no wall}}}{\beta_N^{\text{ideal wall}} - \beta_N^{\text{no wall}}}.$$

The case of $\Omega = 0.0075$ is also computed and full stabilization is obtained. From this figure one can see that the rotation and kinetic stabilization channel appears first near the ideal wall stability limit as the rotation frequency increases. This can be understood from the energy picture introduced in [3]. Using the no wall and ideal wall energy integrals δW_∞ and δW_b, the resistive wall mode growth rate can be written as follows:

$$\gamma \sim -\frac{\delta W_\infty^r \delta W_b^r + \delta W_\infty^i \delta W_b^i}{|\delta W_b^r|^2 + |\delta W_b^i|^2}, \quad (4)$$

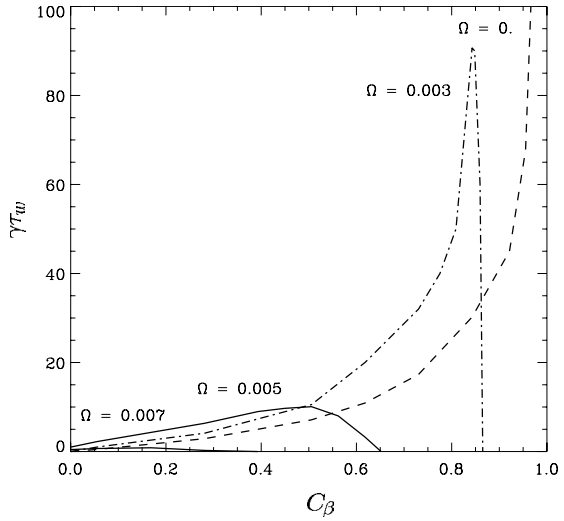

Figure 7. Resistive wall mode growth rate versus the normalized beta C_β for wall position $b = 1.5$, as computed by the AEGIS-K code. The dashed–dot curve represents the growth rate without plasma rotation and kinetic effects. The dashed curve represents the growth rate without plasma rotation and kinetic effects. The dashed–dot ($\Omega = 0.003$), dashed–dot–dot ($\Omega = 0.005$) and solid ($\Omega = 0.007$) curves are the growth rates with plasma rotation and kinetic effects included.

where the superscripts 'r' and 'i' represent the real and imaginary parts, respectively. Without the rotation and kinetic effects ($\delta W^{\rm i}_\infty = \delta W^{\rm i}_b = 0$), the resistive wall mode growth rate tends to infinity at the ideal wall limit $\delta W^{\rm r}_b = 0$. In the presence of the rotation and kinetic effects ($\delta W^{\rm i}_\infty \delta W^{\rm i}_b \neq 0$), the numerator of equation (4) shows that $\delta W^{\rm r}_b = 0$ is also the point which is easiest to be stabilized by the rotation and kinetic effects through resonance induced imaginary part energy $\delta W^{\rm i}_\infty \delta W^{\rm i}_b$.

From figures 6 and 7, one can see that the rotation and kinetic effects may increase the growth rate of the resistive wall modes under the lower end of the stabilization window. The increasing part of the resistive wall mode growth rate in the presence of rotation and kinetic effects resembles the increasing feature of the resistive wall mode growth rate in the ideal MHD description and in the absence of rotation. The stability window near the ideal wall limit is opened as if the ideal MHD resistive wall mode growth rate is suppressed downwards and pushed leftwards (i.e. towards the no wall limit). As a result, the resistive wall mode growth rate under the lower end of the stabilization window increases in the presence of rotation and kinetic effects. This seems to be a typical feature of the stabilization of resistive wall modes through the particle and shear Alfvén resonances as described by equation (4).

In figures 6 and 7 the growth rate curves for $\Omega = 0.003$ decrease sharply. This can also be understood by equation (4). Near the ideal wall limit $\delta W^{\rm r}_b \to 0$, the denominator of equation (4) becomes very small (one order smaller than the first term in the numerator) and consequently the growth rate becomes very large. However, as the system approaches the ideal wall limit, the destabilizing first term in the numerator becomes small as well and the stabilizing second term in the numerator emerges as the dominant term. This changes the growth rate sign and brings down the large growth rate sharply.

4. Conclusions and discussion

In this paper we find that $n = 1$ resistive wall modes in the ITER advanced scenario can be fully stabilized by modestly low rotation. This is achieved at the normalized rotation frequency of $\Omega = 0.0075$ at the magnetic axis with rotation profile $\Omega(1 - \psi^2)$. The existence of this stabilization scheme is proved with the AEGIS-K code, which provides a fully kinetic (non-hybrid) and self-consistent (non-perturbative) description of the system. The wave–particle resonances, shear Alfvén continuum damping, trapped particle effect and parallel electric effects are all taken into account. In our ordering scheme the FLR effects, especially the precessional drift [5], have not been considered. Although the lower range of our parameter domain in figures 6 and 7 approaches the ion diamagnetic drift frequency, the rotation frequency for full stabilization, 0.0075, is well above the diamagnetic drift frequency. Hence, neglecting the FLR effects is justified. Our results represent the first self-consistent theoretical proof of full rotation stabilization.

Our analysis is developed from first principles, namely the Vlasov and Maxwell equations with a suitable ordering scheme. This analysis is enabled by our newly derived gyrokinetic formalism in [9], which recovers MHD in the proper limit and retrieves the missing FLR effects. We note especially that the gyrophase-averaged gyrokinetic equation to lowest order, on which our analysis is based, is different from the conventional drift kinetic equation. As shown in [9], the coupling between the gyrophase-dependent and gyrophase-independent parts of the distribution function must be taken into account in order to derive the drift kinetic equation.

The neutral beam power is relatively small in ITER, and consequently, beam driven rotation could be relatively small. However, there is some uncertainty about the value of the rotation in ITER, since the so-called spontaneous rotation may occur. The C-Mod results show that spontaneous rotation speed is about 10% of the ion thermal speed [14], which is not small. Therefore, the rotation stabilization window found in our paper could be of interest for ITER.

We note the importance of studying the case with even lower rotation frequency, where the precessional drift resonance occurs [5, 6]. However, we believe the theoretical understanding of the precessional drift resonance effect on resistive wall mode stabilization and its experimental validation are still open to question. Reference [6] (numerical proof of [5]) is based on a perturbative method, whereas the non-perturbative hybrid calculations with the MARS-K code show that the perturbative and non-perturbative results differ dramatically [15]. Furthermore, the MARS-K code has not taken into account the finite orbit size and the parallel electric field, among other things. Also, as we have found with our newly developed gyrokinetic theory, the FLR effects have been oversimplified in previous studies. In addition to these reasons, we are also concerned about the numerical scheme and code validation for studies at lower frequencies. Due to the complexity of this problem, one could easily lose the MHD benchmark point in the non-perturbative calculations and no longer be able to identify the MHD eigen mode trace as computed from existing MHD codes such as GATO and AEGIS. For our subsequent investigations, we hope to use

the current results as a starting benchmark point. Indeed, comparison of our MHD (figure 4) and kinetic (figure 5) eigen modes reveals the MHD trace. This frequency domain is easier to benchmark (with the use of the Z-function). And this is another reason why we are pushing this research forward slowly and deliberately.

The other feature of this investigation is the adaptive nature of the AEGIS-K code. From the eigen function given in figure 5 one can see that the radial resolution is an important issue for kinetic computation. It is more challenging than the shear Alfvén continuum damping calculation. In most cases, the radial grid density for output can run as high as 800 with packing at the resonance surfaces. The matrix size in the AEGIS-K numerical scheme is determined by the poloidal Fourier components. Increasing the radial resolution is not accompanied by an increase in the matrix size. This gives the AEGIS-K code the capacity to resolve singular layer behaviour in the presence of kinetic and shear Alfvén resonances.

Although the AEGIS-K numerical scheme is effective and advanced, the AEGIS-K code is still new. Further improvement is likely. We plan to extend the AEGIS-K code to the non–up–down symmetric case and also to include the precession drift resonance together with the FLR effects. The direct comparison with the existing codes such as MARS-K [15] is also under consideration. These will be carried out in the future.

Acknowledgments

This research was supported by the Office of Fusion Energy Science of the US Department of Energy under Grant DE-FG02-04ER54742. The numerical computation is implemented at the United States National Energy Research Scientific Computing Center.

References

[1] Freidberg J.P. 1987 *Ideal Magnetohydrodynamics* (Oxford: Clarendon)
[2] Bondeson A. and Ward D.J. 1994 *Phys. Rev. Lett.* **72** 2709
[3] Betti R. and Freidberg J.P. 1995 *Phys. Rev. Lett.* **74** 2949
[4] Zheng L.J., Kotschenreuther M. and Chu M. 2005 *Phys. Rev. Lett.* **95** 255003
[5] Hu B. and Betti R. 2004 *Phys. Rev. Lett.* **93** 105002
[6] Hu B., Betti R. and Manickam J. 2005 *Phys. Plasmas* **12** 057301
[7] Antonsen T.M. Jr and Lane B. 1980 *Phys. Fluids* **23** 1205
[8] Catto P.J., Tang W.M. and Baldwin D.E. 1981 *Plasma Phys.* **23** 639
[9] Zheng L.J., Kotschenreuther M.T. and Van Dam J.W. 2007 *Phys. Plasmas* **14** 072505
[10] Zheng L.-J., Chu M.S. and Chen L. 1999 *Phys. Plasmas* **6** 1217
[11] Zheng L.J. and Kotschenreuther M. 2006 *J. Comput. Phys.* **211** 748
[12] Zheng L.J., Kotschenreuther M.T. and Van Dam J.W. 2009 AEGIS-K code for linear kinetic analysis of toroidally axisymmetric plasma stability *J. Comput. Phys.* submitted
[13] Bernard L.C., Helton F.J. and Moore R.W. 1981 *Comput. Phys. Commun.* **24** 377
[14] Rice J.E. *et al* 1998 *Nucl. Fusion* **38** 75
[15] Liu Y., Chu M.S., Chapman I.T. and Hender T.C. 2008 *Phys. Plasmas* **15** 112503